A High-Performance Continuously Tunable MEMS Bandpass Filter at 1 GHz

Yonghyun Shim, *Student Member, IEEE*, Zhengzheng Wu, *Student Member, IEEE*, and Mina Rais-Zadeh, *Member, IEEE*

***Abstract*—This paper reports a continuously tunable lumped bandpass filter implemented in a third-order coupled resonator configuration. The filter is fabricated on a Borosilicate glass substrate using a surface micromachining technology that offers high-Q tunable passive components. Continuous electrostatic tuning is achieved using three tunable capacitor banks, each consisting of one continuously tunable capacitor and three switched capacitors with pull-in voltage of less than 40 V. The center frequency of the filter is tuned from 1 GHz down to 600 MHz while maintaining a 3-dB bandwidth of 13%–14% and insertion loss of less than 4 dB. The maximum group delay is less than 10 ns across the entire tuning range. The temperature stability of the center frequency from -50°C to 50°C is better than 2%. The measured tuning speed of the filter is better than 80 μs, and the $\mathrm{IIP_3}$ is better than 20 dBm, which are in good agreement with simulations. The filter occupies a small size of less than 1.5 cm $\times$ 1.1 cm. The implemented filter shows the highest performance amongst the fully integrated microelectromechanical systems filters operating at sub-gigahertz range.**

***Index Terms*—Micromachining, passive filters, RF microelectromechanical systems (MEMS), tunable bandpass filters, tunable capacitors, UHF filters.**

I. Introduction

THERE IS an increasing demand for high-performance RF front-end modules for advanced ground mobile radios. With the introduction of joint tactical radios as the next-generation system in the U.S. military, ground mobile radios have to support various waveforms, including VHF and UHF bands, which will require reconfigurable RF front-ends [1]. The key challenge in developing reconfigurable RF front-end modules is to reduce the size and weight while supporting multiple communication standards [2]. As the key component of the RF front-end, the band-select filter needs to satisfy the above-mentioned requirements, namely, multiple frequency band coverage and good RF performance, all in a small form factor. This calls for a single fully integrated frequency-tunable bandpass filter.

In the VHF or UHF range, lumped *LC* filters offer the smallest size compared to other alternative implementations such as cavity filters [3], [4] and distributed filters [5]–[7]. Using conventional CMOS technology, the size of the filter could be significantly reduced. However, the quality factor (Q) of CMOS-based passives is low, making it hard to achieve a sufficiently low insertion loss for the bandpass filter unless Q enhancement techniques using active components are utilized [8]. The power-handling capability of CMOS varactors is also limited, further constraining their application in RF systems [9]. Microelectromechanical systems (MEMS) technology can lead to low insertion-loss tunable filters with high RF power-handling capability, meeting all the requirements of ground mobile radios.

There are a few reports on tunable bandpass filters having all integrated components centered at frequencies below 1 GHz [10], [11]. The reported filters are designed in the second-order coupled resonator configuration. Due to the low order of the filter, the shape factor and out-of-band rejection of these filters are limited. In addition, in these filter implementations, a large-value fixed capacitor is placed in parallel with a smaller-value MEMS capacitor to obtain the required capacitance value, reducing the tuning range of the filters to less than 25%. In this paper, a continuously tunable MEMS bandpass filter using a third-order coupled resonator configuration is proposed. Using continuous tuning, the frequency of the filter can be tuned to select any desired frequency in the tunable frequency range or altered to account for fabrication inaccuracies. Continuous tuning is achieved using MEMS tunable capacitors that exhibit high Q's (exceeding 100), fast tuning speed (less than 80 μs), wide capacitance tuning range (5:1), and good temperature stability [12], [13].

DC and RF characteristics of the tunable capacitor plays an important role in defining the characteristics of the filter, such as the tuning range, tuning speed, power handling, and power consumption. Among different actuation mechanisms, electrostatic tuning is most commonly used because of its low power consumption [14]. A problem with electrostatic tuning is the pull-in effect, which limits the travel range of the moving element. The tuning range of electrostatic capacitors can be improved by using a capacitor gap smaller than the actuation gap. Such capacitors, called dual-gap capacitors, can exhibit high tuning ratios exceeding 5:1 and are employed in this work to tune the frequency [12], [13].

Two-port capacitors are commonly used for matching or as the coupling elements in coupled resonator filters [15]. Using capacitive matching and coupling, it is hard to maintain a fixed bandwidth without tuning the value of the coupling capacitors. In this work, mutually coupled inductors and inductive

Manuscript received October 19, 2011; revised April 19, 2012; accepted April 23, 2012. Date of publication June 05, 2012; date of current version July 30, 2012. This work was supported by the Harris Corporation under the Wide Tuning Range Integrated Filter for Tactical Radios Project and by the National Science Foundation (NSF) under Grant 1055308.

The authors are with the Electrical Engineering and Computer Science Department, The University of Michigan at Ann Arbor, Ann Arbor, MI 48109 USA (e-mail: yhshim@umich.edu; zzwu@umich.edu; minar@umich.edu).

Color versions of one or more of the figures in this paper are available online at http://ieeexplore.ieee.org.

Digital Object Identifier 10.1109/TMTT.2012.2198228

TABLE I
TARGET SPECIFICATIONS OF THE PROPOSED FILTER

Filter Characteristics	Target
Center frequency range	600 MHz ~ 1000 MHz
Insertion loss	< 4 dB at ω_c
3dB-Bandwidth (BW_{3dB})	12 ~ 16 % of ω_c
Shape factor (BW_{30dB} / BW_{3dB})	< 4
Passband ripple	< 0.5 dB
Out-of-band rejection	> 40 dB
Group delay	< 10 ns
Impedance	50 Ω
IIP_3	> 20 dBm
Tuning voltage	< 50 V
Tuning speed	< 100 μs
Temperature variation (ω_c)	< 5 %
Dimensions	< 1.5 × 1.5 cm^2

matching are utilized to provide a wider band matching and avoid complicated tuning control. Using broadband inductive matching and wide-range capacitive tuning in the resonator, a tunable filter is demonstrated with insertion loss of less than 4 dB and tuning range of 40%. To our best knowledge, this is the first single-chip implementation of a third-order tunable filter at sub-gigahertz range, which addresses diverse aspects of filter performance, such as insertion loss, tuning range, shape factor, linearity, tuning speed, and temperature stability.

This paper is organized as follows. First, the design and tuning configuration of the filter are discussed. Next, the design of each passive component and their 3-D electromagnetic simulation results are shown. The linearity analysis for the 1-dB compression point (P1 dB) and the third-order intermodulation intercept point (IIP_3) are also described. Finally, the measurement and characterization results of the fabricated filter are presented.

II. TUNABLE BANDPASS FILTER DESIGN

The target specifications of the pre-select tunable filter are listed in Table I. The filter is aimed to achieve frequency coverage from 600 MHz to 1 GHz with a 3-dB percentage bandwidth of 13%–14%. The insertion loss of the filter is targeted to be less than 4 dB to achieve a small noise figure for the entire radio. To obtain a shape factor (30-dB bandwidth $(\mathrm{BW}_{30\ \mathrm{dB}})$ to 3-dB bandwidth $(\mathrm{BW}_{3\ \mathrm{dB}})$) of less than 4, the order of the filter needs to be at least 3 [16]. A third-order Chebyshev filter with a 0.5-dB passband ripple is selected to achieve the desired shape factor. Using this configuration, the group delay is less than 10 ns, meeting all the specifications listed in Table I.

The filter design procedure is as follows. First, the low-pass prototype in Chebychev configuration is designed. The low-pass prototype values (g_1, g_2, g_3, g_4) of the third-order Chebyshev filter used here are 1.5963, 1.0967, 1.5963, and 1.0000, respectively. The low-pass filter (LPF) is then converted to a coupled resonator bandpass filter configuration using admittance inverters, as shown in Fig. 1(a). With this configuration, values of the lumped components are easily realizable using MEMS surface micromachining technologies [10]. The parameters of the

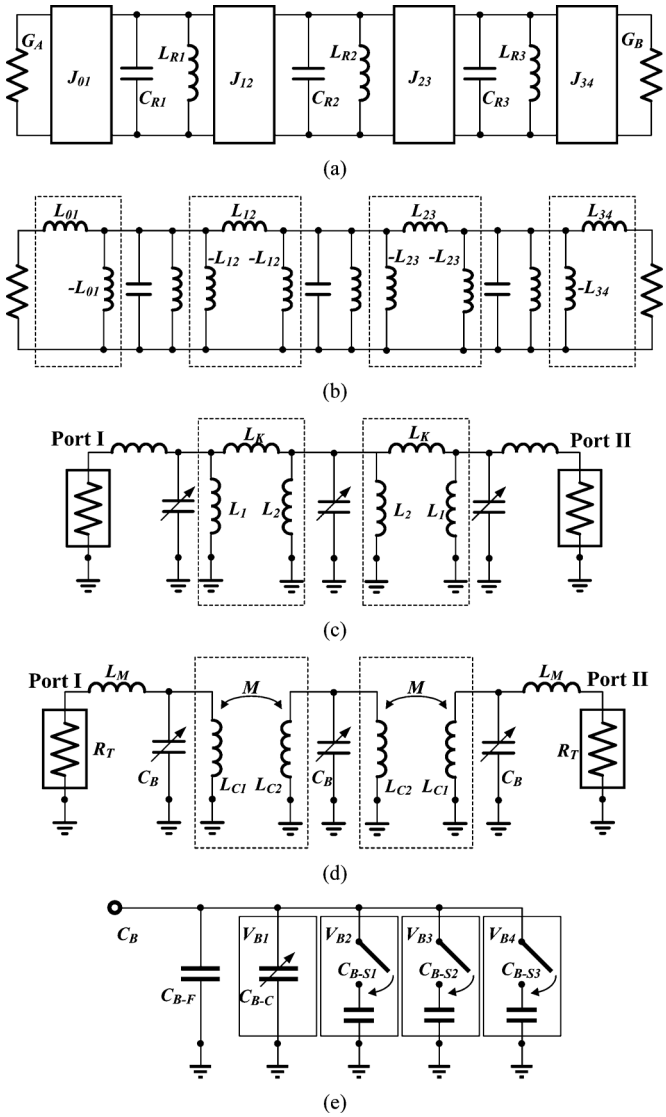

Fig. 1. Schematic views showing the design procedure of the third-order bandpass filter in this work. (a) Generalized bandpass filter using admittance inverter. (b) Conversion into inductive coupling. (c) Arrangement of inductance for mutual-inductive coupling. (d) Final schematic view of the filter. (e) Detail composition of the tunable bank included in each resonator.

admittance inverters are derived using the following equations [17]:

$$J_{01} = J_{34} = \frac{1}{2\pi f_c} \cdot \frac{1}{\sqrt{g_0 g_1 G_A L_{R1}}} \tag{1}$$

$$J_{12} = J_{23} = \frac{1}{2\pi f_c} \cdot \frac{\mathrm{BW}_{3\ \mathrm{dB}}}{f_c} \cdot \frac{1}{\sqrt{g_1 g_2 L_{R1} L_{R2}}} \tag{2}$$

where f_c is the center frequency of the bandpass filter at initial state, G_A is the input impedance, and L_{R1} and L_{R2} are inductor values in each LC tank. To ease the characterization and tuning scheme, the initial value of all three capacitors (C_{R1}, C_{R2}, C_{R3}) are set to be the same. An initial value of 2.3 pF is chosen for the tunable capacitors, considering that the inductance value needs to be in the range of 1–15 nH to provide a high Q of more than 40. Using these values for the capacitors, the required inductance value for $L_{R1}, L_{R2},$ and L_{R3} is 11 nH and the unloaded Q_0 of each resonator would be about 40.

As shown in Fig. 1(b), the admittance inverter is implemented using inductive coupling with $L_{12} = L_{23} = 1/(2\pi f_c J_{12})$. Values of L_{01} and L_{34} are not set at this step as they also depend on the matching condition.

The equivalent inductor of the second resonator $(-L_{12}//L_{R2}//-L_{23})$ in Fig. 1(b) is split into two inductors [L_2's in Fig. 1(c)]. In Fig. 1(c), L_1 in the first and third resonators can be approximated as $L_{R1}//(-L_{12})$. To achieve more feasible inductance values, the inductive π-network of Fig. 1(c) is converted into mutually coupled inductors, as shown in Fig. 1(d). The matching inductance (L_M) is derived considering g_1 and g_4 and the loaded Q_n of the resonator. The mutual inductance (M) and resonator inductances ($L_{C1}\prime$, $L_{C2}\prime$) are derived from L_1, L_2, and L_K using well-known equations in [16].

To obtain the effective impedance of g_1 and g_4 at input and output nodes and impedance matching to 50 Ω, impedance transformation using two inductors (L_{C1}, L_M) in Fig. 1(d) is obtained using the following expressions:

$$L_{C1} = \frac{L_M L_{C1}^{'} R_S}{R_S\left(L_M - L_{C1}^{'}\right) + R_T L_{C1}^{'}} \quad L_M = \frac{\sqrt{R_S R_T}}{2\pi f_c} \tag{3}$$

$$L_{C2} \approx L_{C2}^{'} \quad R_S = \frac{2\pi f_c \cdot L_{R1} Q_0 \cdot L_{R1} Q_n}{L_{R1} Q_0 - L_{R1} Q_n} \tag{4}$$

where R_T is the target input impedance (50 Ω) and R_S is the input impedance looking into the resonator.

To achieve frequency tuning, a tunable capacitor bank, which consists of one fixed capacitor (MIM capacitor), one continuously tunable capacitor, and three capacitive switches [see Fig. 1(e)], is employed in each resonator section. The tuning control mechanism is as follows. First the continuously tunable capacitor is tuned. When this capacitor reaches its maximum value, a switch will be turned ON and the value of the continuously tunable capacitor will be reset to set the frequency as required. To further tune the center frequency, again the continuously tunable capacitor will be tuned to finally reach its maximum value. At this state, another switch will be turned on. Therefore, to achieve continuous tuning, only one continuously tunable capacitor is required. Other capacitors are switched to ease the tuning control. The initial capacitance value of all tunable capacitors is set to 200 fF with tuning bias of less than 40 V, and tuning speed of less than 80 μs including the stabilization time. The capacitance value and the corresponding filter frequency range at each tuned state are listed in Table II. The mechanical design of the tunable capacitors is reported elsewhere [12]. The values of the passive components in Fig. 1 are listed in Table III. In Section III, the simulation results and 3-D electromagnetic layout of the filter are presented.

TABLE II
TUNING CONFIGURATION

Tuning Controls	Capacitance (C_B)	Center Frequency (f_C)
V_{B1} = 0-40 V	2.3-3.5 pF	811-1000 MHz
V_{B1} = 0-40 V V_{B2} = 40 V	3.4-4.6 pF	707-824 MHz
V_{B1} = 0-40 V V_{B2} , V_{B3} = 40 V	4.5-5.7 pF	635-715 MHz
V_{B1} = 0-40 V V_{B2} , V_{B3} , V_{B3} = 40 V	5.6-6.8 pF	582-640 MHz

TABLE III
DESIGN VALUES OF THE MEMS FILTER

Symbol	Description	Value
J_{01}, J_{34}	Admittance inverter parameters	8.49e-6
J_{12}, J_{23}	Admittance inverter parameters	1.75e-3
L_1	Inductively coupled inductor 1	12.5 nH
L_2	Inductively coupled inductor 2	29.0 nH
L_K	Coupling inductor	90.9 nH
L_M	Matching inductor	32.0 nH
L_{C1}	Mutually coupled inductor 1	16.4 nH
L_{C2}	Mutually coupled inductor 2	22.6 nH
M	Mutual inductance	3.2 nH
R_T	Target Input / Output Impedance	50
C_B	Tunable capacitor bank (TCB)	2.3 pF ~ 6.8 pF
$C_{B\text{-}F}$	Fixed capacitor in TCB	1.5 pF
$C_{B\text{-}C}$	Continuous capacitor in TCB	0.2 pF ~ 1.4 pF
$C_{B\text{-}S}$	Switched capacitor in TCB	0.2 pF ~ 1.3 pF

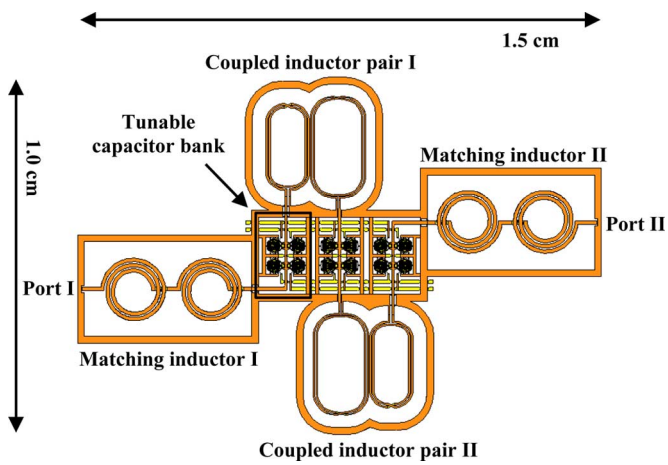

Fig. 2. Layout of the MEMS tunable filter.

III. 3-D ELECTROMAGNETIC SIMULATION

Filters are designed and fabricated using a multiple-metal surface micromachining process technique [18]. This technology offers three metal layers (0.5 μm Au/4 μm Au/40 μm Cu), one dielectric layer [aluminum oxide (Al_2O_3)] and two sacrificial layers (PMMA/Shipley 1813 photoresist). Using this process, each tunable or fixed passive component can be optimized for the highest performance with a selection of metals, dielectrics, and sacrificial layers. The performance of individual passive components, as well as the tunable filter, is simulated using the ANSOFT HFSS 3-D electromagnetic simulation tool [19]. The material properties, such as conductivity, dielectric constant, and loss tangent, are characterized and the extracted values from measurements are used in the simulations.

The integrated filter layout is shown in Fig. 2. The detailed design of the matching inductor and coupled inductor is discussed in [18]. The lengths of the RF interconnecting lines are minimized and the ground connections are optimally placed to

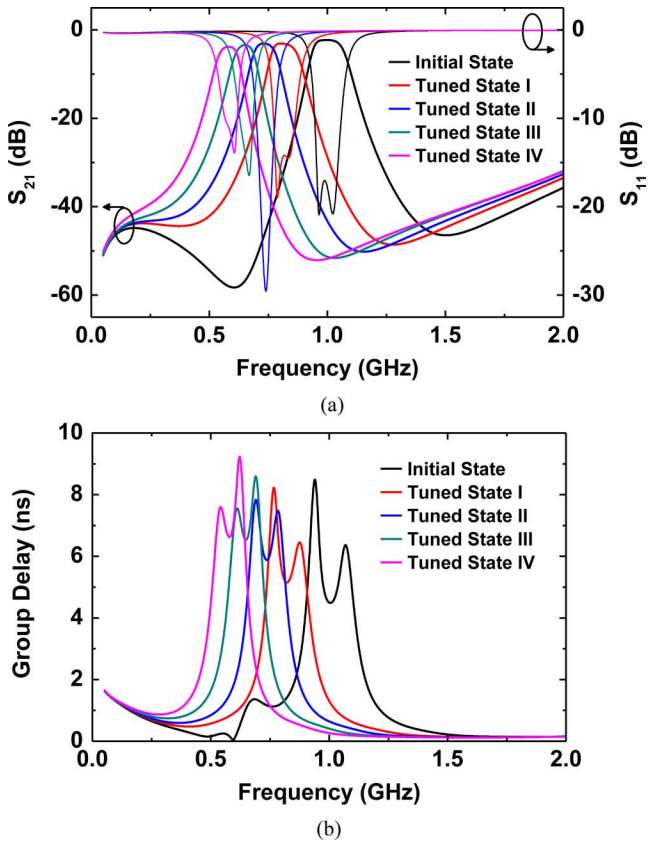

Fig. 3. Simulation results of the MEMS filter. (a) S-parameters. (b) Group delay.

TABLE IV
SIMULATED FILTER SPECIFICATIONS USING HFSS 3-D EM TOOL

Tuned Capacitors	Insertion Loss	3dB Bandwidth	Shape Factor	Group Delay
No tuning	2.3 dB @ 1005 MHz	139 MHz (13.8 %)	3.1	< 9 ns
Tuning_1	3.2 dB @ 825 MHz	120 MHz (14.5 %)	3.5	< 9 ns
Tuning_2	3.1 dB @ 734 MHz	102 MHz (13.9 %)	3.8	< 8 ns
Tuning_3	3.4 dB @ 650 MHz	90 MHz (13.8 %)	4.1	< 9 ns
Tuning_4	3.8 dB @ 580 MHz	92 MHz (15.9 %)	4.1	< 10 ns

reduce loss and parasitics. The bias lines of the three tunable capacitors in each resonator tank are connected together. One bias line also controls all corresponding capacitive switches. Therefore, only one analog bias line and three digital (0 V/40 V) bias lines are needed to tune the filter (instead of 12 control lines).

The HFSS simulated insertion loss, return loss, and group delay of the integrated filter at each tuned state are shown in Fig. 3. In the simulations, nonideal conditions such as reduced capacitance tuning range and additional loss from the substrate are reflected from the characterization results of the tunable capacitor banks and the inductors [18]. The group delay in Fig. 3(b) is derived using the formula suggested in [20]. The simulated performance of the filter is summarized in Table IV.

TABLE V
PARAMETERS OF THE VARACTOR USED IN NONLINEAR SIMULATIONS

Symbol	*Description*	*Value*
C_{S0}	Initial capacitance in sensing node	200 fF
C_{A0}	Initial capacitance in actuation node	220 fF
g_{S0}	Initial air gap in sensing node	0.5 μm
g_{A0}	Initial air gap in actuation node	2.0 μm
f_m	Mechanical resonant frequency	22 kHz
k	Spring constant	75 N/m
Q_M	Mechanical quality factor	2

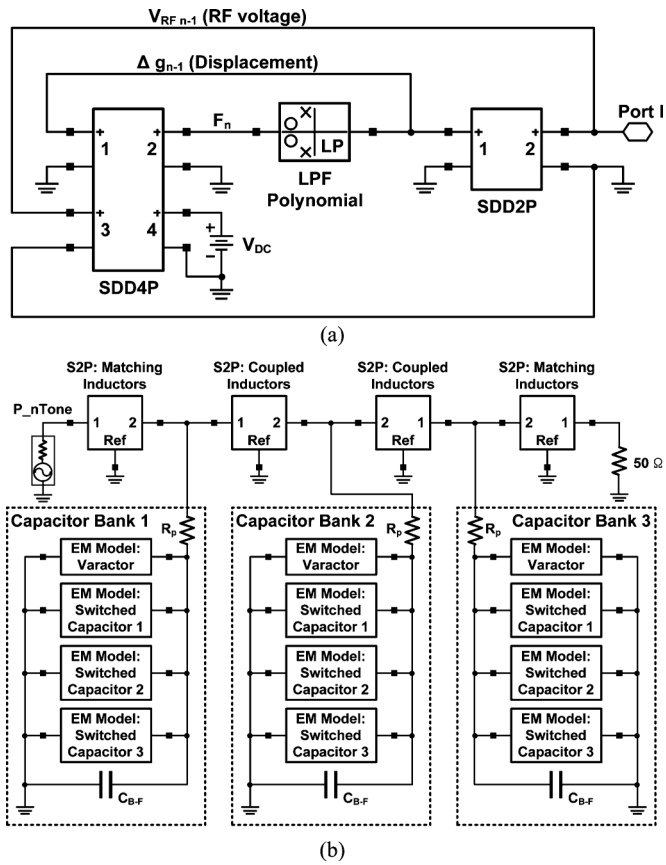

Fig. 4. Schematic view of the nonlinear electromechanical model for the: (a) varactor and (b) entire filter.

IV. LINEARITY ANALYSIS

The Agilent ADS simulation tool is used to analyze the nonlinear performance of the filters [21]. To estimate the P1 dB and IIP_3 values, the nonlinearity of the varactor and capacitive switches are taken into account using nonlinear electromechanical (EM) models [22]. The simulation parameters such as initial capacitance, air gap, and mechanical properties of the varactor are summarized in Table V. All values are carefully extracted from HFSS electromagnetic simulations and modal/displacement analysis in ANSYS [23].

Since the integrated varactor has separate electrodes for actuation and capacitance sensing, the total force can be approximated as the sum of actuation force from dc bias applied to the actuation electrode and the RF self-actuation force from the capacitance sensing electrode. Since the varactor has a dual-gap configuration, the equations in [22] are modified to take into

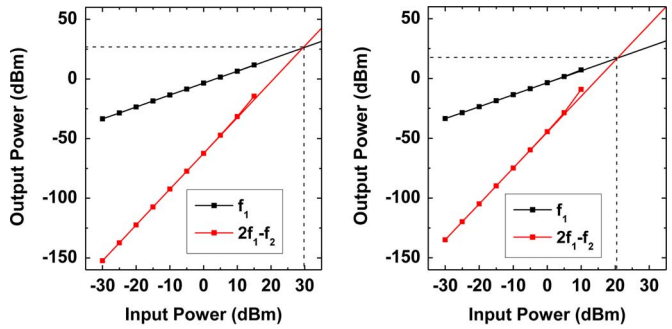

Fig. 5. IIP_3 value extracted from the nonlinear electromechanical model at frequency offset of 20 kHz: (a) without dc bias and (b) with 25 V of dc bias.

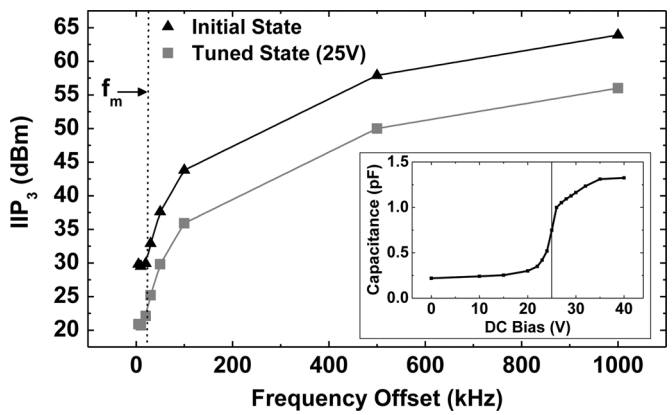

Fig. 6. IIP_3 value extracted from the nonlinear electromechanical model at different frequency offsets with and without dc bias. Tuning characteristics of the tunable capacitor is shown in the inset.

account both the sense and actuation gaps. The following equations are applied to the EM model of the varactor in Fig. 4(a) in order to calculate the nth-iterated total force applied to the top membrane and the sense capacitance, respectively,

$$F_n = \left(C_{S0} \cdot \frac{g_{S0}}{g_{S0} - \Delta g_{n-1}}\right) \cdot \left(\frac{V^2_{\mathrm{RF}\ n-1}}{2(g_{S0} - \Delta g_{n-1})}\right) + \left(C_{A0} \cdot \frac{g_{A0}}{g_{A0} - \Delta g_{n-1}}\right) \cdot \left(\frac{V^2_{\mathrm{DC}}}{2(g_{A0} - \Delta g_{n-1})}\right) \quad (5)$$

$$C_{Sn} = C_{S0} \cdot \frac{g_{S0}}{g_{S0} - \Delta g_n} = C_{S0} \cdot \frac{g_{S0}}{g_{S0} - (F_n/k)} \quad (6)$$

where Δg_{n-1}, $V_{\mathrm{RF}\ n-1}$, and V_{DC} are the change of air gap and the equivalent RF bias from the $(n-1)$th iteration, and the dc tuning bias, respectively.

As shown in Fig. 4(a), a four-port symbolically defined device (SDD4P) is utilized to implement (5), where the value of Port 2 output, F_n, is derived from the other three port values, Δg_{n-1}, $V_{\mathrm{RF}n-1}$, and V_{DC}. Likewise, an SDD2P on the right side is utilized to calculate the value of Port 2 output, C_{Sn}, from the Port 1 input value, Δg_n, using (6). The LPF polynomial reflects the mechanical response of the MEMS capacitor with parameters f_m, k, and Q_m. The schematic of the filter configuration taking into account the nonlinear models of the varactor and switched capacitors is shown in Fig. 4(b). The initial air gap at the sensing node is set as 1.5 μm.

Fig. 5 shows the harmonic simulation result at different input power levels. The frequency difference of the two input tones is

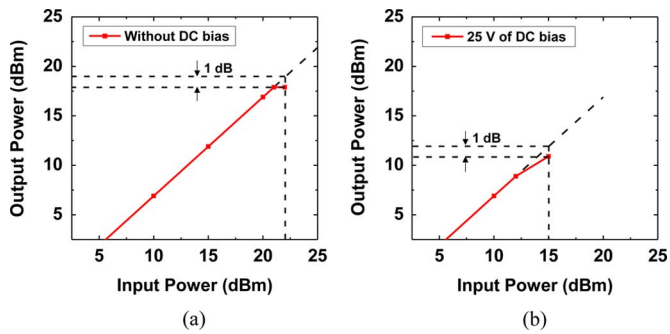

Fig. 7. P1 dB value extracted from the nonlinear electromechanical model: (a) without dc bias and (b) with 25 V of dc bias.

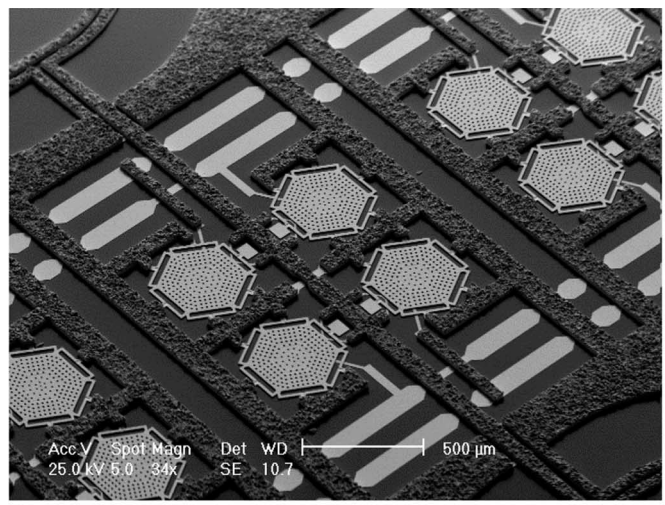

(a)

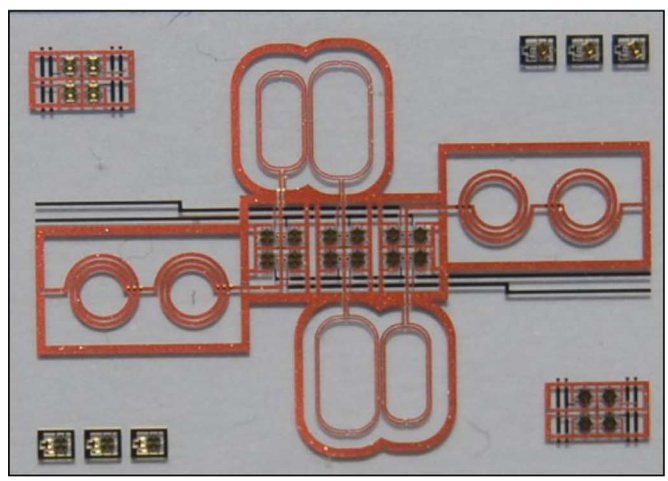

(b)

Fig. 8. (a) Scanning electron microscope (SEM) view. (b) Photographic view of a fabricated filter.

20 kHz. The extracted IIP_3 value is 30 dBm when no dc bias is applied to the varactors/switches. With the application of 25-V dc bias, the IIP_3 is reduced to 20 dBm. At this bias point, the capacitance value of the varactors is most sensitive to the applied RF power as the C–V curve has the sharpest slope at this point (see inset of Fig. 6). Therefore, 20 dBm is a pessimistic estimation of IIP_3 when a dc bias is applied. The extracted IIP_3 at different input frequency offsets is shown in Fig. 6. At both

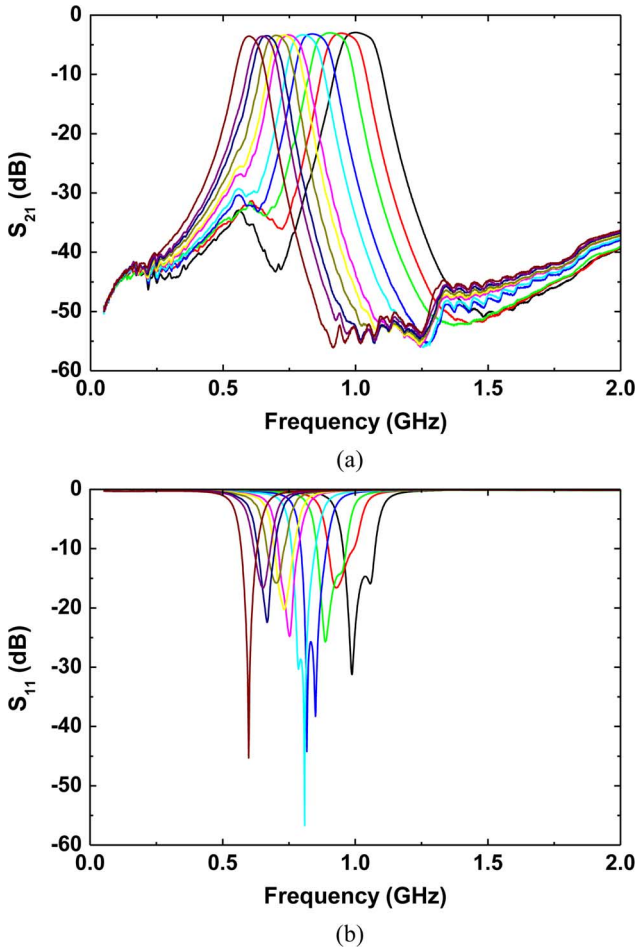

Fig. 9. Measured filter response at each tuned stage. (a) Insertion loss. (b) Return loss.

initial and tuned states, the IIP_3 value is better for larger frequency offsets. This is due to the low-pass filtering behavior of the MEMS capacitors, which is taken into account in the nonlinear EM model of Fig. 4(a) by considering a cutoff frequency of 22 kHz (the mechanical resonant frequency (f_m) of the tunable capacitor). A similar trend is expected in the measured IIP_3.

The P1 dB is also simulated using the same EM models. Fig. 7(a) and (b) shows the simulated P1 dB when 0 and 25 V of actuation bias are applied, respectively. The extracted P1 dB is 22 dBm when no dc bias is applied to the varactors/switches, whereas it is reduced to 15 dBm when 25 V of dc bias is applied. The power-handling capability of these filters is thus limited to P1 dB and not to the IIP_3 value.

V. Measurement Result

Insertion loss and return loss are measured using Cascade Microtech ground–signal–ground (GSG) ACP probes and an N5214A Agilent PNA-X network analyzer. The dc bias is applied to each bias line using Microtech dc probes. The images of the fabricated device are shown in Fig. 8. The footprint of the entire filter is around 1.5 cm × 1.0 cm, which is much smaller than other UHF filters using microstrip lines and SMT passive components [5]–[7].

TABLE VI
Measured Filter Specifications at Each Tuned Stage

Tuned Capacitors	Insertion Loss	3dB Bandwidth	Shape Factor	Group Delay
No tuning	3.0 dB @ 1011 MHz	135 MHz (13.4 %)	3.2	< 7 ns
Tuning_1	3.3 dB @ 833 MHz	113 MHz (13.6 %)	4.5	< 8 ns
Tuning_2	3.4 dB @ 735 MHz	99 MHz (13.5 %)	4.6	< 9 ns
Tuning_3	3.6 dB @ 650 MHz	87 MHz (13.4%)	4.7	< 9 ns
Tuning_4	3.6 dB @ 602 MHz	81 MHz (13.5 %)	4.7	< 8 ns

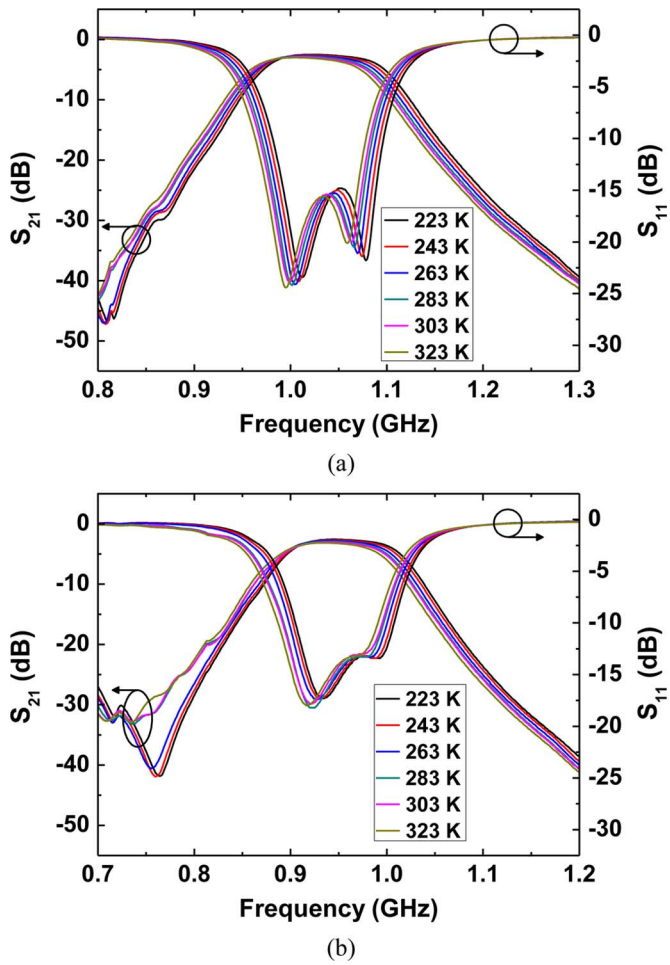

Fig. 10. Measured filter response at different temperatures. (a) At initial state. (b) When a dc bias of 25 V is applied to C_{B-C}.

A. Insertion Loss and Return Loss

Fig. 9 shows the measured insertion loss and return loss at each tuned state when dc bias of 0 to 40 V is applied to the varactors and switched capacitors. The center frequency is tuned from an initial value of 1011–602 MHz by applying a maximum of 40 V to the capacitors. Across the entire tuning range, the insertion loss is less than 4 dB and the return loss is greater than 15 dB. The measurement results are summarized in Table VI. The 3-dB bandwidth shows good agreement with the electromagnetic simulation. However, the measured shape factor at most tuned states is above 4. This is caused by an unwanted

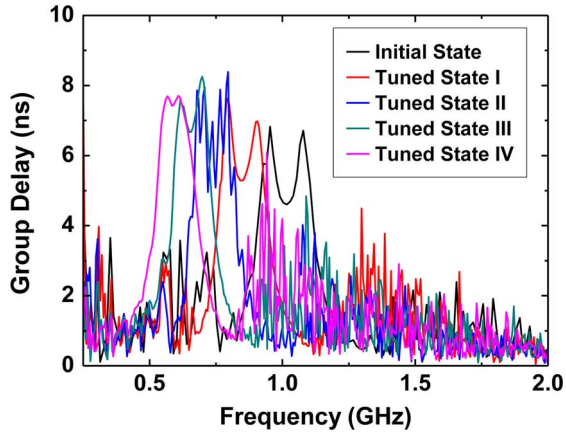

Fig. 11. Measured group delay at each tuned stage.

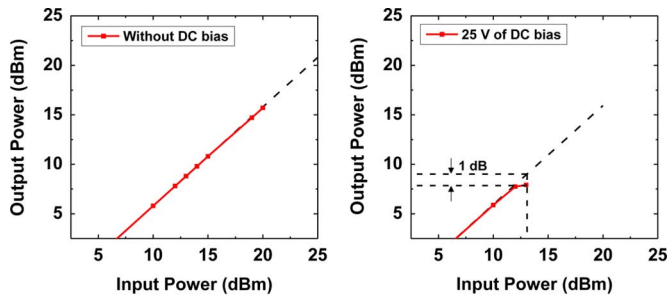

Fig. 12. Measured input power versus output power. (a) Without dc bias. (b) With 25 V of dc bias.

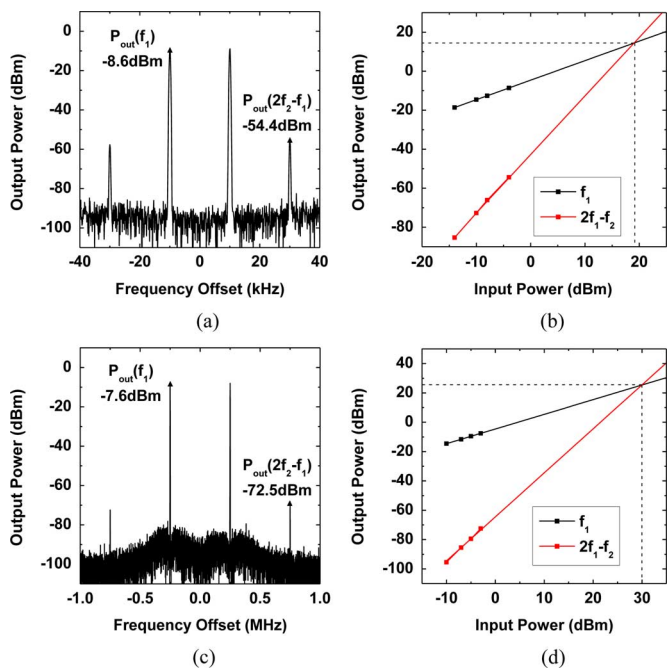

Fig. 13. Measured power spectrum when 25 V of dc bias is applied to the continuously tunable capacitor. (a) Output power spectrum with frequency offset of 20 kHz and input power of −4 dBm. (b) Extracted IIP_3 with frequency offset of 20 kHz. (c) Output power spectrum with frequency offset of 500 kHz and input power of −3 dBm. (d) Extracted IIP_3 with frequency offset of 500 kHz.

resonance located at the lower side of the passbands. This resonance is presumably due to the coupling between the inductors

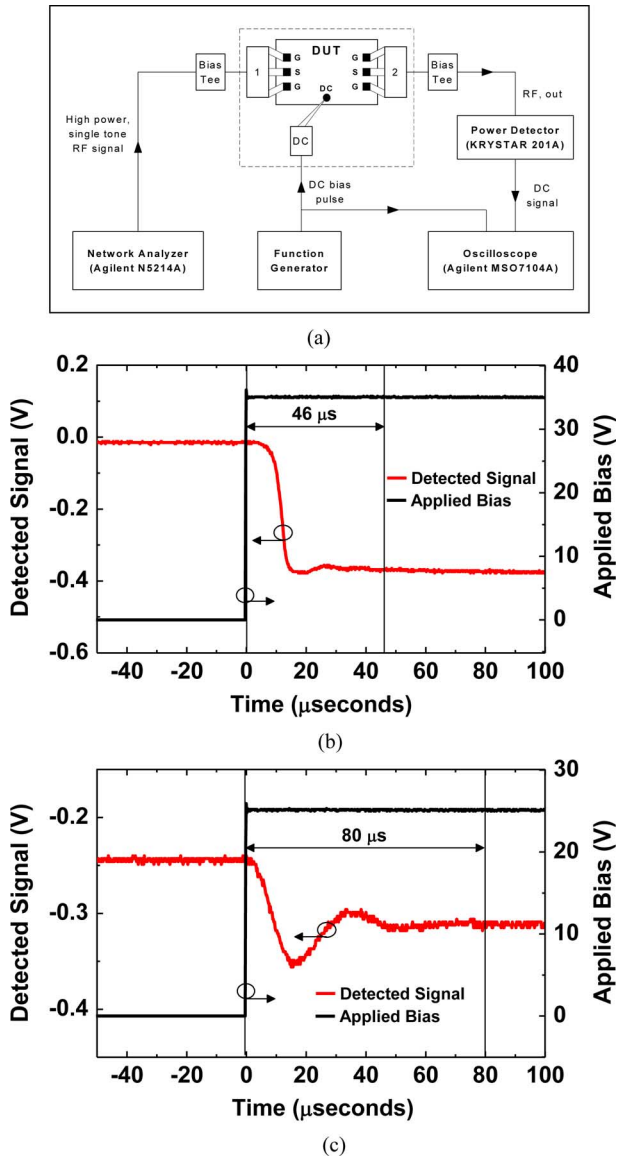

Fig. 14. (a) Setup used for tuning-speed measurements. The measured tuning speed when: (b) 40 V and (c) 25 V is applied to continuously tunable capacitor, respectively.

and the ground plane on the backside of the wafer and can be reduced by increasing the thickness of the substrate (i.e., 500-μm thick).

Temperature stability of the filter is tested using a Microtech KV-230 cryogenic station and GGB RF probes. Short-open-load-thru (SOLT) calibration is done at each temperature. Fig. 10(a) shows the filter response from −50 °C to 50 °C when no dc bias is applied. The center frequency of the filter is shifted from 1035 to 1016 MHz, showing a variation of less than 2%. The frequency response of the filter when a dc bias is applied to one of the capacitors is shown in Fig. 10(b). Upon temperature change, the center frequency is shifted by 1.5% from 955 to 941 MHz, which is considered small for a MEMS device [24], [25]. The temperature stability of the filter is better than the temperature shift of the varactor itself. The capacitance variation of individual varactors is less than 7% over the same temperature range [12]. Since the varactor is placed in parallel with a more temperature stable fixed capacitor, the

TABLE VII
COMPARISON BETWEEN TUNABLE FRONT-END FILTERS IN THE UHF RANGE

	Brown '00 [5]	Manuel '05 [6]	Rais-Zadeh '09 [10]	Xiu '10 [7]	*This work*
f_c	700-1330 MHz	470-862 MHz	786-836 MHz	680-1000 MHz	602-1011 MHz
Filter configuration	5th order discretely tunable combline filter	3rd order continuously tunable combline filter	2nd order continuously tunable lumped filter	2nd order continuously tunable combline filter	3rd order continuously tunable lumped filter
Insertion loss	2.0-6.0 dB	3.0-6.0 dB	4.0-6.0 dB	1.1-1.5 dB	3.0-3.6 dB
BW_{3dB}	8-22 % of f_c	1-3 % of f_c	5-6 % of f_c	8-12 % of f_c	13-14 % of f_c
BW_{30dB}/BW_{3dB}	2.0-3.0	3.0-5.0	> 7.0	5.0-6.0	3.2-4.7
Tuning Speed	N/A	< 1 μs	< 1 ms	< 1 μs	40-80 μs
IIP_3	18-24 dBm	N/A	N/A	13 dBm	20-30 dBm
Technology	PCB + MEMS switch	PCB + CMOS varactor	MEMS (single chip)	PCB + CMOS varactor	MEMS (single chip)
Size	< 31.0 × 40.0 mm^2	< 50.0 × 65.0 mm^2	< 5.0 × 6.0 mm^2	< 30.0 × 30.0 mm^2	< 11.0 × 15.0 mm^2

temperature stability of the filter is improved at the initial state, as well as the tuned state of the varactors.

B. Group Delay

The group delay of the filter at each tuned state is extracted from the measured S-parameters. As shown in Fig. 11, the group delay is less than 10 ns, meeting the design requirement.

C. Linearity

The P1 dB measurements are carried out using an N5214A Agilent PNA-X network analyzer in the high-power narrowband detection mode, which supports up to 20 dBm of input source power. Fig. 12(a) shows the measured input power versus output power with zero dc bias. As expected from the simulations shown in Fig. 7(a), the filter shows no significant degradation up to 20 dBm of input power. The measured P1 dB with 25 V of dc bias is around 13 dBm [see Fig. 12(b)], which is similar to the simulated value in Fig. 7(b).

The IIP_3 measurements are carried out in the two-tone source power mode. As the IIP_3 of the PNA-X receiver itself is around 30 dBm, IIP_3 values higher than 30 dBm cannot be accurately measured using this system. Therefore, the IIP_3 of the filter without dc bias could not be measured; it was only verified that the IIP_3 value is above 30 dBm at both 20 and 500 kHz of frequency offset.

Fig. 13(a)–(d) shows the linearity measurements when 25 V of dc bias is applied to the varactor. When dc bias is applied, IIP_3 degrades as the smaller capacitance gap becomes more sensitive to the RF signal power. As shown, the IIP_3 value is at the lowest at 20 kHz of frequency offset, i.e., the mechanical resonance frequency of the varactor membrane. The extracted IIP_3 at 20-kHz offset is about 20 dBm [see Fig. 13(b)], which is close to the simulated value of 22 dBm shown in Fig. 5(b). The IIP_3 with an applied voltage of 25 V at 500-kHz frequency offset is also above 30 dBm [see Fig. 13(d)].

D. Tuning Speed

The tuning speed of the filter is measured using the setup shown in Fig. 14(a). 10 dBm of a single-tone RF signal at the corresponding center frequency for the dc tuning bias is applied using the network analyzer. The RF signal at the output port is converted into dc voltage using a KRYTAR 201A power detector. The RF signal before applying the bias is zero; after application of bias, the filter tunes to the frequency of the input RF signal and a nonzero power is detected using the power detector. The tuning bias and power detector outputs are monitored with an Agilent MSO7104A oscilloscope to extract the tuning speed.

Fig. 14(b) shows transition of detected power level when a pull-in bias of 40 V is applied to the tunable capacitors. The measured transition time with this bias condition is better than 50 μs, which is the maximum tuning speed of the filter. As shown in Fig. 14(c), with 25 V of dc bias, the transition time is around 80 μs. At this bias, the membrane does not completely touch down and the stabilization time is longer.

E. Comparison

There has been extensive work on tunable front-end filters in the UHF band, implemented with several different configurations and integration methods. For successful adoption in the RF front-end system, a filter should satisfy wide frequency band coverage, low insertion loss, and high power-handling capability, all in a small size and low cost. Filter implementations using integration of passives with varactor diodes or employing MEMS capacitors on a printed circuit board (PCB) can satisfy only a few of these requirements [5]–[7] (Table VII). Integration of separately packaged passives can not only result in additional insertion loss, but also derive increased fabrication cost and size. The form factor of a reported filter fabricated using a single-chip MEMS technology [10] is much smaller than that implemented using the PCB technology. However, its tuning performance was limited due to the low order of the filter, and limited tuning range of the tunable capacitors. In this work, a significantly better performance is achieved using 12 wide-tuning range MEMS capacitors and a higher order filter in a Chebyshev configuration. Compared to the reported work, the filter presented in this paper is the highest performance single-chip filter in the sub-gigahertz frequency band.

VI. CONCLUSION

Design and measurements of a continuously tunable MEMS bandpass was reported in this paper. Insertion loss of the filter at all tuned states (from 600 MHz to 1 GHz) is less than 4 dB, while the 3-dB bandwidth is maintained within 13%–14 %. The shape factor of the filter is above 4 (less than 5) and can be improved by optimizing the layout of the inductors and reducing the substrate coupling. The measured shift in center frequency of the filter is less than 1.5% across 100 °C of temperature change and the tuning speed is better than 80 μs. The worst case IIP_3 is around 20 dBm. However, considering the lower value of P1 dB, the practical range of power is limited to about 13 dBm.

Improvements in the design of tunable capacitors are required to achieve better power-handling capability. Future work will focus on such design optimizations, as well as characterization of other filter specifications such as phase noise and sensitivity to vibration. The presented filter technology could be extended to other applications in the UHF range such as TV tuners, which requires smaller channel selection bandwidth.

REFERENCES

[1] R. North, N. Browne, and L. Schiavone, "Joint tactical radio system-connecting the GIG to the tactical edge," in *IEEE Military Commun. Conf.*, Oct. 23–25, 2006, pp. 1–6.

[2] M. S. Hasan, M. LaMacchia, L. Muzzelo, R. Gunsaulis, L. T. C. R. Housewright, and J. Miller, "Designing the joint tactical radio system (JTRS) handheld, manpack, and small form fit (HMS) radios for interoperable networking and waveform applications," in *IEEE Military Commun. Conf.*, Oct. 29–31, 2007, pp. 1–6.

[3] H. Joshi, H. H. Sigmarsson, S. Moon, D. Peroulis, and W. J. Chappell, "High-Q fully reconfigurable tunable bandpass filters," *IEEE Trans. Microw. Theory Tech.*, vol. 57, no. 12, pp. 3525–3533, Dec. 2009.

[4] S. Park, I. Reines, C. Patel, and G. M. Rebeiz, "High-Q RF-MEMS 4–6-GHz tunable evanescent-mode cavity filter," *IEEE Trans. Microw. Theory Tech.*, vol. 58, no. 2, pp. 381–389, Feb. 2010.

[5] A. R. Brown and G. M. Rebeiz, "A varactor-tuned RF filter," *IEEE Trans. Microw. Theory Tech.*, vol. 48, no. 7, pp. 1157–1160, Jul. 2000.

[6] M. Sanchez-Renedo, R. Gomez-Garcia, J. I. Alonso, and C. Briso-Rodriguez, "Tunable combline filter with continuous control of center frequency and bandwidth," *IEEE Trans. Microw. Theory Tech.*, vol. 53, no. 1, pp. 191–199, Jan. 2005.

[7] X. Y. Zhang, Q. Xue, C. H. Chan, and B. Hu, "Low-loss frequency-agile bandpass filters with controllable bandwidth and suppressed second harmonic," *IEEE Trans. Microw. Theory Tech.*, vol. 58, no. 6, pp. 1557–1564, Jun. 2010.

[8] S. Bantas and Y. Koutsoyannopoulos, "CMOS active-LC bandpass filters with coupled-inductor Q-enhancement and center frequency tuning," *IEEE Trans. Circuits Syst. II, Exp. Briefs*, vol. 51, no. 2, pp. 69–76, Feb. 2004.

[9] R. R. Mansour, S. Fouladi, and M. Bakeri-Kassem, "Integrated RF MEMS/CMOS devices," in *Design, Test, Integration, Packag. MEMS/MOEMS Symp.*, Apr. 9–11, 2008, pp. 374–375.

[10] M. Rais-Zadeh, H. M. Lavasani, A. Kapoor, and F. Ayazi, "An integrated 800-MHz coupled-resonator tunable bandpass filter in silver with a constant bandwidth," *J. Microelectromech. Syst.*, vol. 18, no. 4, pp. 942–949, Aug. 2009.

[11] Y. Shim, R. Tabrizian, F. Ayazi, and M. Rais-Zadeh, "Low-loss MEMS bandpass filters with improved out-of-band rejection by exploiting inductive parasitics," in *IEEE Int. Electron Devices Meeting*, Dec. 7–9, 2009, pp. 1–4.

[12] Y. Shim, Z. Wu, and M. Rais-Zadeh, "A high-performance, temperature-stable, continuously tuned MEMS capacitor," in *IEEE Int. MEMS Conf.*, Jan. 23–27, 2011, pp. 752–755.

[13] Y. Shim, J. Ruan, Z. Wu, and M. Rais-Zadeh, "An integrated RF MEMS tunable filters," in *IEEE Int. MEMS Conf.*, Jan. 29–Feb. 2, 2012, pp. 15–18.

[14] D. Peroulis and L. P. B. Katehi, "Electrostatically-tunable analog RF MEMS varactors with measured capacitance range of 300%," in *IEEE MTT-S Int. Microw. Symp. Dig.*, Jun. 8–13, 2003, vol. 3, pp. 1793–1796.

[15] M. Rais-Zadeh, "Wafer-level encapsulated high-performance MEMS tunable passives and bandpass filters," Ph.D. dissertation, Dept. Elect. Eng., Georgia Inst. Technol., Atlanta, GA, 2008.

[16] A. I. Zverev, *Handbook of Filter Synthesis*. New York: Wiley, 2005.

[17] G. Matthaei, E. M. T. Jones, and L. Young, *Microwave Filters, Impedance-Matching Networks, and Coupling Structures*. New York: McGraw-Hill, 1964.

[18] Y. Shim, Z. Wu, and M. Rais-Zadeh, "Three-metal surface-micromachining for high-yield tunable capacitors and high-Q inductors," *J. Microelectromech. Syst.*, accepted for publication.

[19] HFSS. ver. 12, ANSYS Inc., Canonsburg, PA, 2009. [Online]. Available: http://www.ansoft.com/products/hf/hfss/

[20] I. Shapir, "Suggestion for a new formula to calculate group-delay from frequency domain measurements," in *Eur. Microw. Conf.*, Sep. 2006, pp. 1233–1236.

[21] ADS 2009. Agilent Technol., Santa Clara, CA, 2009. [Online]. Available: http://www.agilent.com/find/eesof-ads/

[22] L. Dussopt and G. M. Rebeiz, "Intermodulation distortion and power handling in RF MEMS switches, varactors, and tunable filters," *IEEE Trans. Microw. Theory Tech.*, vol. 51, no. 4, pp. 1247–1256, Apr. 2003.

[23] ANSYS. ver. 12, ANSYS Inc., Canonsburg, PA, 2009. [Online]. Available: http://www.ansys.com/

[24] H. Nieminen, V. Ermolov, S. Silanto, K. Nybergh, and T. Ryhanen, "Design of a temperature-stable RF MEM capacitor," *J. Microelectromech. Syst.*, vol. 13, no. 5, pp. 705–714, Oct. 2004.

[25] I. Reines, B. Pillans, and G. M. Rebeiz, "Thin-film aluminum RF MEMS switched capacitors with stress tolerance and temperature stability," *J. Microelectromech. Syst.*, vol. 20, no. 1, pp. 193–203, Feb. 2011.

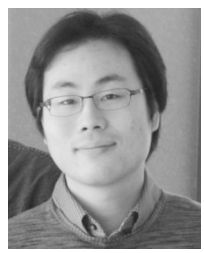

Yonghyun Shim (S'09) received the B.S. degree in electrical engineering from Seoul National University, Seoul, Korea, in 2007, the M.S.E. degree in electrical engineering and computer science from The University of Michigan at aAnn Arbor, in 2009, and is currently working toward the Ph.D. degree in electrical engineering and computer science at The University of Michigan at Ann Arbor.

His research interests include micromachined RF front-end filters, RF MEMS passives, RF integrated circuits (ICs) and wireless front-ends, and CMOS-MEMS integration.

Zhengzheng Wu (S'09) received the B.S. degree in microelectronics from Fudan University, Shanghai, China, in 2005, the M.S. degree in microelectronics from the Shanghai Institute of Microsystem and Information Technology, Chinese Academy of Sciences, Shanghai, China, in 2009, and is currently working toward the Ph.D. degree in electrical engineering and computer science at The University of Michigan at Ann Arbor.

During Summer 2011, he was an Intern with Samsung Telecommunications America, Dallas, TX, where he was involved in the development of multiband RF power amplifiers for wireless handsets. His research interests include MEMS for wireless applications and timing references, tunable RF filters and passive circuits, circuits for wireless transceivers, and integrated microsystems.

Mr. Wu was the recipient of the Rackham International Student Fellowship of The University of Michigan at Ann Arbor for 2010–2011. He was a Student Paper Competition finalist of the 2011 IEEE Microwave Theory and Techniques Society (IEEE MTT-S) International Microwave Symposium (IMS).

Mina Rais-Zadeh (S'03–M'08) received the B.S. degree in electrical engineering from the Sharif University of Technology, Tehran, Iran, in 2002, and the M.S. and Ph.D. degrees in electrical and computer engineering from the Georgia Institute of Technology, Atlanta, in 2005 and 2008, respectively.

From August 2008 to 2009, she was a Postdoctoral Research Fellow with the Integrated MEMS Group, Georgia Institute of Technology. Since January 2009, she has been with The University of Michigan at Ann Arbor, where she is currently an Assistant Professor with the Department of Electrical Engineering and Computer Science. Her research interests include passive micromachined devices for communication applications, resonant micromechanical devices, gallium–nitride MEMS, and microfabrication/nanofabrication process development.

Prof. Rais-Zadeh is a member of the Technical Program Committee of the IEEE IEDM, IEEE Sensors, and Hilton Head Workshop. She was the recipient of the National Science Foundation (NSF) CAREER Award (2011) and the IEEE Electron Device Society Early Career Award (2011). She was a finalist in the Student Paper Competition of the SiRF (2007) and IMS (2011) conferences.